

COMPUTATIONAL INVESTIGATIONS OF THE TRANSMEMBRANE ITALIAN-MUTANT (E22K) $3A\beta_{11-40}$ IN AQUEOUS SOLUTION

SON TUNG NGO^{a,b,†}

^aComputational Chemistry Research Group,
Ton Duc Thang University, Ho Chi Minh City, Vietnam

^bFaculty of Applied Sciences,
Ton Duc Thang University, Ho Chi Minh City, Vietnam

[†]E-mail: ngosontung@tdtu.edu.vn

Received 14 July 2018

Accepted for publication 26 August 2018

Published 11 September 2018

Abstract. *The Amyloid beta A(β) oligomers are characterized as critical cytotoxic materials in Alzheimer's disease (AD) pathogenesis. Structural details of transmembrane oligomers are inevitably necessary to design/search potential inhibitor to treat AD. However, the experimental detections for structural information of low-order A β oligomers are precluded due to the extremely dynamic fluctuation of the oligomers. In this project, the transmembrane Italian-mutant (E22K) $3A\beta_{11-40}$ (tmE22K $3A\beta_{11-40}$) was extensively investigated using the temperature replica exchange molecular dynamics (REMD) simulations. The structural changes of the trimer when replacing the negatively charged residue E22 by a positively charged residue K were monitored over simulation intervals. The oligomer size turned to be larger and the increase of β -content was recorded. The momentous gain of intermolecular contacts with lipid molecules implies that tmE22K $3A\beta_{11-40}$ would be self-inserted more easily into the membrane than the wild-type (WT) form. Furthermore, the tighter interaction between constituting monomers was indicated implying that the E22K mutation probably enhances the A β fibril formation. The results are in good agreement with experiments showing that E22K amyloid self-aggregates faster than the WT form. Detailed information of tmE22K trimer structure and kinetics probably yield the understanding of AD mechanism.*

Keywords: amyloid oligomer, E22K, Italian mutation, REMD, transmembrane.

Classification numbers: 87.10.Tf; 87.15.ap; 33.15.Bh; 87.14.ep.

I. INTRODUCTION

There are several millions of people under effects of Alzheimer's disease (AD) worldwide [1, 2]. The amyloid is indicated as the most important factor causing the AD [3, 4]. Although there are several failures in design of AD drug targeting Amyloid beta ($A\beta$) peptides [5, 6], the Amyloid cascade hypothesis is still supported by numerous scientists [7, 8]. The reasons for the drug designed failure have just been proposed [9]. In particular, the neurotoxic elements are $A\beta$ oligomers instead of monomers or fibrils [10, 11], which locate in a mixture environments involving much of various forms of $A\beta$ peptides such as oligomers and fibrils [12]. Furthermore, the structures of low-weight $A\beta$ oligomers, known to be more cytotoxic, are extremely dynamic fluctuating between various states [13]. The experimental detections for structures of low-weight $A\beta$ oligomers are thus prohibited. The lacking information of $A\beta$ oligomer shapes in experiments much reduces the efficient AD therapy. Since the $A\beta$ self-aggregations *in silico* are in good agreement with experiments, computational studies have been performed to provide more details in understanding these processes [4].

As mentioned above, details of $A\beta$ oligomer structures are necessary for screening the AD inhibitors [14, 15]. Replacing a residue in the hydrophobic core may alter the self-assembly of $A\beta$ peptides. Indeed, the familial mutations on the central hydrophobic region of N-terminal lead to extreme effects on the shapes of $A\beta$ oligomer including A21G [16], E22Q [17], E22G [18], E22 Δ [19], and D23N [20]. Especially, modifying negatively charged residue E by a positively charged residue K greatly alters the fibril formations [21, 22]. Numerous investigations were thus carried out to determine the altering self-oligomerization of the $A\beta$ peptides [22, 23]. In addition, it is known that the toxicity of $A\beta$ oligomers is associated with their interaction with the neuron cell membrane. Upon the binding of $A\beta$ oligomers to the membrane, the calcium ion homeostasis is amended, resulting in the death of neuron cells [24, 25]. Although the large transmembrane $A\beta$ systems consisting of many monomers were estimated by using atomic force microscopy [26], obtaining the experimental picture of the transmembrane low-weight $A\beta$ oligomers is an obstacle. The mission is often completed using computational methods recently [27]. Computational evaluations of the effect of mutant E22K on the conformations of the transmembrane $3A\beta_{11-40}$ peptide are of great interests since $A\beta$ trimer is one of the most neuro-harmful elements [12].

In this work, the temperature replica exchange molecular dynamics (REMD) simulations with the length of 400 ns involving 32 various replicas were carried out to evaluate the structural alteration of the transmembrane mutant E22K $3A\beta_{11-40}$ (*tmE22K* $3A\beta_{11-40}$). In particular, the *tmE22K* $3A\beta_{11-40}$ was entirely embedded into the dipalmitoyl phosphatidylcholine (DPPC) lipid bilayers in aqueous solution. Obtained results demonstrated that the kinetic and structural properties of *tmE22K* $3A\beta_{11-40}$ are seriously different from the transmembrane wild-type $3A\beta_{11-40}$ (*tmWT* $3A\beta_{11-40}$) [28]. Upon the simulations, the oligomer size is evaluated through analyzing gyration of radius (R_g), surface area (SA), and collision cross section (CCS). The secondary structure of E22K trimer is monitored upon define secondary structure of proteins (DSSP) protocol. The optimized conformations of *tmE22K* trimer were acquired utilizing the combination of free energy landscape (FEL) and clustering methods. The outcome of computational results produces the features of *tmE22K* trimer shapes and how contrast these features are from those of *tmWT* $3A\beta_{11-40}$ [28]. The understanding may help us to advance more closely in research of AD therapy.

II. MATERIALS AND METHODS

II.1. Starting structure of the *tmE22K* $3A\beta_{11-40}$ peptide

The $3A\beta_{11-40}$ peptide was obtained from the two-fold $12A\beta_{11-40}$ fibril [29]. The peptide was mutated at the residue E22 utilizing PyMOL mutagens tool [30]. The united-atom force field named GROMOS 53a6 [31] was served to represent the *tmE22K* $3A\beta_{11-40}$ citing previous studies [27,28]. The *tmE22K* $3A\beta_{11-40}$ peptide was then inserted into the DPPC lipid bilayer [32]. Finally, the transmembrane system was solvated using SPC water model [33]. In particular, the initial conformation of the soluble *tmE22K* $3A\beta_{11-40}$ peptide consists of 125 DPPC molecules, 3,293 water molecules, and 3 Cl^- atoms (total atoms of 16,984) as shown in Fig. 1. The size of periodic boundary conditions box is of 6.42 nm \times 6.44 nm \times 7.60 nm.

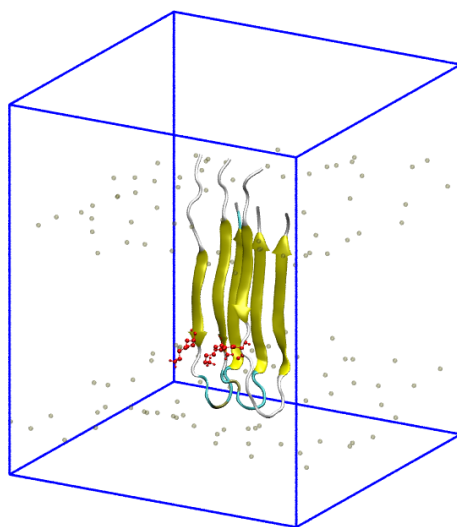


Fig. 1. The starting conformation of the *tmE22K* $3A\beta_{11-40}$. In particular, the E22K mutation residues are highlighted in red color. Tan spheres represent the phosphorus atoms of DPPC membrane lipid bilayer. Solvated molecules are hidden in this figure in order to clarify.

II.2. REMD simulation

The temperature REMD simulations are an extensive method to inspect the folding/misfolding of $A\beta$ peptides [34–37]. In present work, these investigations were carried out using GROMACS version 5.1.3 [38]. In the beginning, the *tmE22K* $3A\beta_{11-40}$ energy was minimized using steepest descent method. The energy minimized system was shortly unwound using 500 ps of NVT simulations, during which the protein atoms were positionally restrained employing a weak harmonic force. The relaxed system was then pretended proving parallel tempering approach with temperatures ranging from 321.00 to 422.58 K (321.00, 323.93, 326.89, 329.86, 332.86, 335.87, 338.92, 341.98, 345.06, 348.17, 351.3, 354.45, 357.63, 360.83, 364.05, 367.3, 370.57, 373.87, 377.19, 380.53, 383.89, 387.28, 390.7, 394.14, 397.6, 401.09, 404.61, 408.15, 411.72, 415.31, 418.94, and 422.58 K). The computational parameters were introduced in the previous study [27,28].

II.3. Measured Tools

The intermolecular side-chain (SC) contact was counted when the minimum distance between non-hydrogen atoms of two residues (of different monomers) is smaller than 4.5 Angstrom. The intermolecular hydrogen bond contact (HB) between various residues (of various monomers) was predicted when the distance between acceptor and donor is smaller than 3.5 Angstrom and the angle between acceptor-hydrogen-donor is larger than 135° [36]. The surface area (SA) and radius of gyration were computed applying GROMACS tools. The secondary structure terms were calculated utilizing DSSP package [39]. The collision cross section (CCS) of the peptide was detected with the help of IMPACT application [40]. The collective variance free energy landscape (FEL) was constructed using the GROMACS tool “sham” with coordinates of root-mean-square deviation (RMSD) and gyration of radius (R_g) [41]. The lipid order specification was calculated as mentioned in previous studies [27, 28].

III. RESULTS AND DISCUSSION

III.1. The *tmE22K* $3A\beta_{11-40}$ Peptide during REMD simulations

The enhance sampling method named REMD simulation is often employed to determine the structural change of amyloid beta peptides [35, 42, 43]. In this work, the structure of *tmE22K* $3A\beta_{11-40}$ was started from fibril-like structure referring to the previous study [27]. The parallel temperature simulations were performed with 32 various replicas with 32 differing temperatures grading from 321.0 to 422.6 K (details in the Materials & Methods section). Each replica was simulated over 400 ns of MD simulations. In total, there are 12,800 ns of MD simulations with the mean exchange rate of 22%. In order to dodge the initial tendency, the first 150 ns of REMD simulation was repealed from any evaluation. The measured values were thus analyzed from the time interval 150-400 ns of REMD simulation at 324 K.

The structure change of *tmE22K* $3A\beta_{11-40}$ over REMD simulation at 324 K was monitored as shown in Fig. 2. When the E22K mutation was induced, the transmembrane trimer forms a larger size and more β -structure in comparison with the *tmWT* system. In particular, the radius of gyration of the *tmE22K* $3A\beta_{11-40}$ is increased by an amount of 8% in comparison with the *tmWT* $3A\beta_{11-40}$ (E22K $R_g \simeq 1.53 \pm 0.05$ nm versus *tmWT* $R_g \simeq 1.42 \pm 0.05$ nm) [28]. In agreement with gyrate radius, the *tmE22K* $3A\beta_{11-40}$ SA (72.20 ± 5.14 nm²) and CCS (14.47 ± 0.74 nm²) are inevitably larger than those of the *tmWT* $3A\beta_{11-40}$ with the corresponding values of 64.73 ± 3.07 and 13.42 ± 0.31 nm² (Table 1), respectively. The β -content of the *tmE22K* $3A\beta_{11-40}$ (44 ± 4 %) is significantly larger than that of *tmWT* $3A\beta_{11-40}$ (40 ± 7 %). The *tmE22K* trimer also adopts a very different RMSD curve from the values of *tmWT* one (Fig. 2). Overall, these contracts imply that *tmE22K* $3A\beta_{11-40}$ has larger structures and are more stable than *tmWT* $3A\beta_{11-40}$ due to forming a larger number of β -content.

III.2. Secondary Structure of the Mutation

As mentioned above, the E22K mutation increases the β -content of transmembrane $A\beta$ trimer (4). It may be argued that *tmE22K* $3A\beta_{11-40}$ apparently stables than the *tmWT* $3A\beta_{11-40}$. Accordingly, the turn/coil-structure of the *tmE22K* $3A\beta_{11-40}$ is smaller than those of the *tmWT* system. Interestingly, the helical structure of the *tmE22K* trimer was lacked in whole simulation trajectory. It is known that the α -content is a transitional state of the $A\beta$ peptides self-assembly

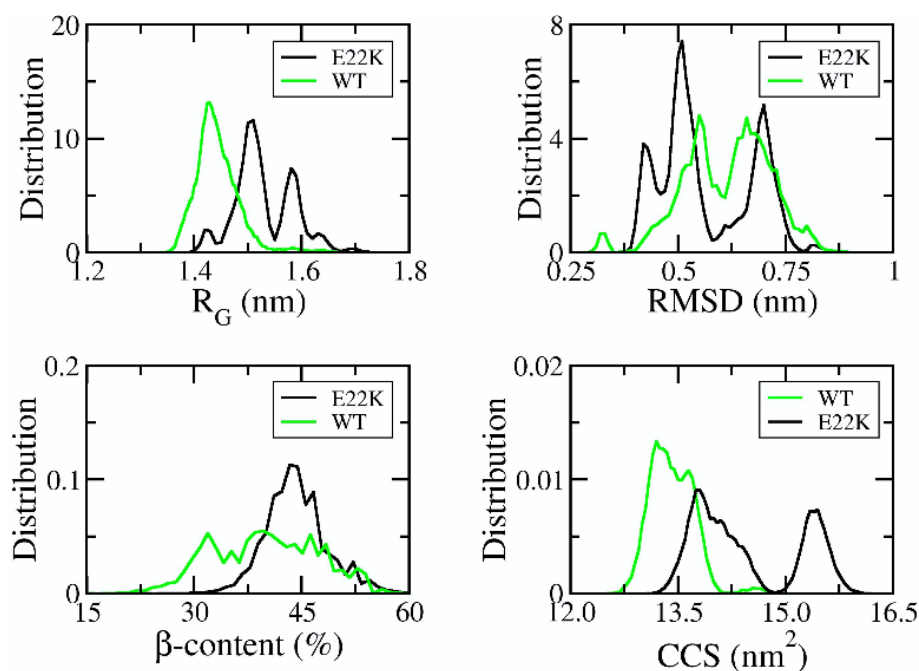


Fig. 2. The distribution of computed metrics of tmE22K 3A β_{11-40} systems during interval 150-400 ns of REMD simulations at 324 K. The metrics of the tmWT 3A β_{11-40} were reproduced from Ref [28] with permission from the Royal Society of Chemistry.

Table 1. The sizes of tmE22K and tmWT 3A β_{11-40} systems were described from R_g , SA, and CCS analyses.

	R_g (nm)	SA (nm ²)	CCS (nm ²)
E22K	1.53 ± 0.05	72.20 ± 5.14	14.47 ± 0.74
WT [#]	1.42 ± 0.02	64.73 ± 3.07	13.42 ± 0.31

[#]The secondary structure metrics of tmWT 3A β_{11-40} was reported in previous study [28].

progress. The lacking of the α -content may imply that the E22K mutation probably enhances the folding rate of A β peptides [44,45].

The per-residue structure terms were also determined as displayed in Fig. 3. All residues can be arranged into five critical patterns as residues 11-13, 22-29, and 38-40 adopting solid coil structure, while residues 14-21 and 30-37 exhibit a large amount of β -structure. The turn content is rarely observed in residues 12-13 and 22-26. Interestingly, the mutant E22K not only enhances the β -structure of residue K22 but also turns residue A21 forming more β -content. Furthermore, especially, the mutant E22K much increases β -structure of C-terminal (residues 30-37). In addition, the α -content is absolutely negligible over the peptide.

Table 2. The average of secondary structure terms of *tmE22K* $3A\beta_{11-40}$ peptides in comparison with WT one. The unit is of percentage (%).

	β -content	α -content	Turn-content	Coil-content
E22K	44 ± 4	0 ± 0	1 ± 1	55 ± 5
WT [#]	40 ± 7	0 ± 1	2 ± 2	57 ± 7

[#]The secondary structure metrics of transmembrane WT $3A\beta_{11-40}$ peptide was reported in previous study [28].

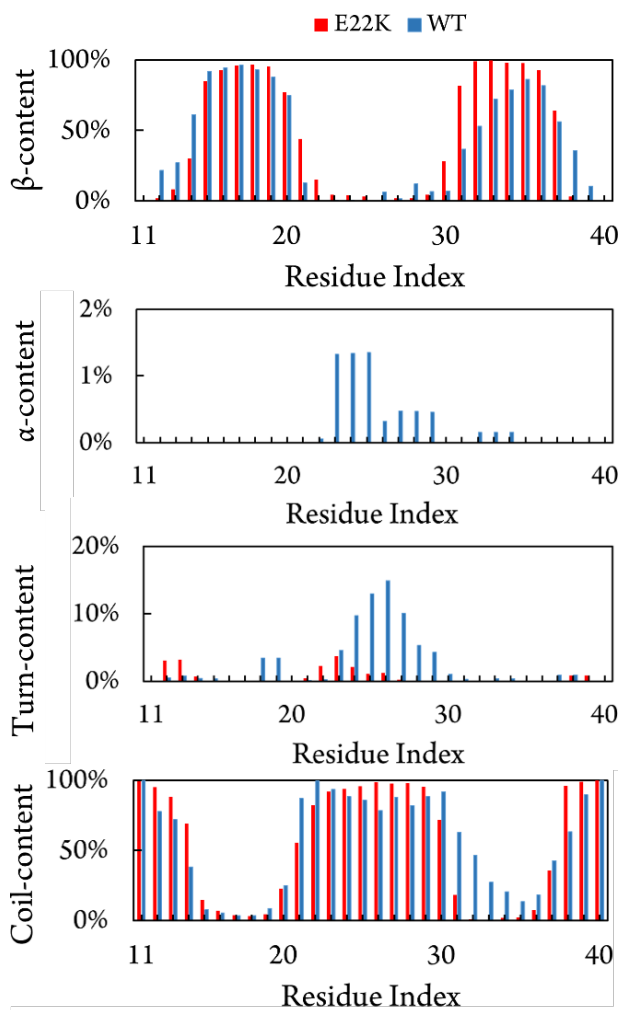


Fig. 3. Secondary structure terms per residue of *tmE22K* and *tmWT* (reproduced from Ref. 28 with permission of the Royal Society of Chemistry) $3A\beta_{11-40}$ peptides.

III.3. The FEL and Optimized Structures of *tmE22K* 3A β_{11-40}

The optimized shapes of the *tmE22K* 3A β_{11-40} were searched utilizing FEL and clustering methods [46], which was prospered to perform this demand [47]. Observed results are described in 5. Most of *tmE22K* 3A β_{11-40} shapes bend in the range of RMSD (from 0.37 to 0.86 nm) and R_g (from 1.39 to 1.74 nm). It is a large shift in comparison with *tmWT* system with the corresponding values range from 0.20 to 0.65 nm of RMSD and from 1.33 to 1.50 nm of R_g [28]. In total, three free energy holes have been observed and noted as **A**, **B**, and **C**. The coordinates of these minima at (RMSD; R_g) are (1.51; 0.50), (1.58; 0.70), and (1.53; 0.43).

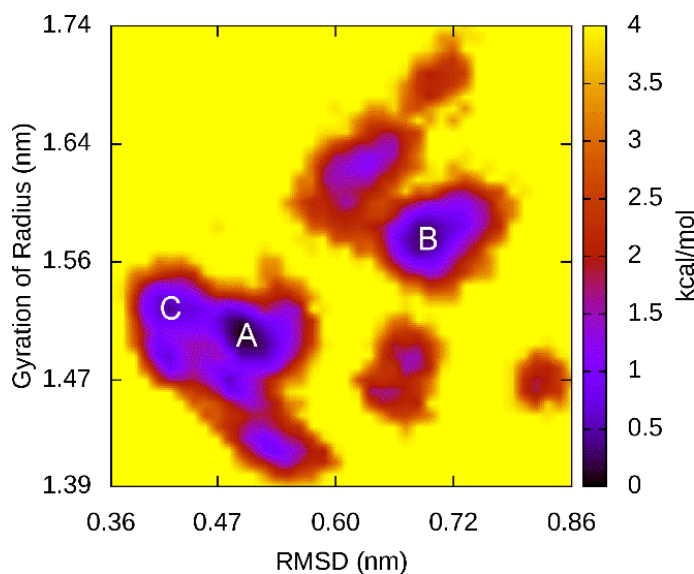


Fig. 4. The FEL of the *tmE22K* 3A β_{11-40} was constructed. In particular, three optimized shapes corresponding to the free energy holes were observed and presented in Fig. 5.

The representative structures of *tmE22K* trimer are obtained and displayed in Fig. 4. The shapes adopt U-shape structural style with strong inter-contact (both SC and HB) between two monomers, resulting in the stable of β -sheet penetrating the membrane. The C-/N-terminal and the loop regions adopt rigid interaction with solvation and surface of DPPC membrane, thus the random coil structure mostly appears in the regions. In particular, details of these shapes are described in Table 3. In particular, the shape **A** drops the largest population with values of 37%, while the populations of conformations **B** and **C** are significantly smaller with amounts of 25 and 16%, respectively. The conformations **A** and **B** form the smallest amount of β -content with a value of 40% in comparison to shapes **C** (44%). Interestingly, the conformation **B** adopts the largest size with corresponding amounts of R_g , SA, and CCS are of 1.59 nm, 79.34 nm², and 15.46 nm², respectively (Table 3). The shape **A** is found with the smallest intensity with the smallest values of R_g (1.51 nm), SA (67.31 nm²), and CCS (nm²). The shape **C** is of medium size with corresponding amounts of 1.53 nm (R_g), 70.76 nm² (SA), and 14.34 nm² (CCS).

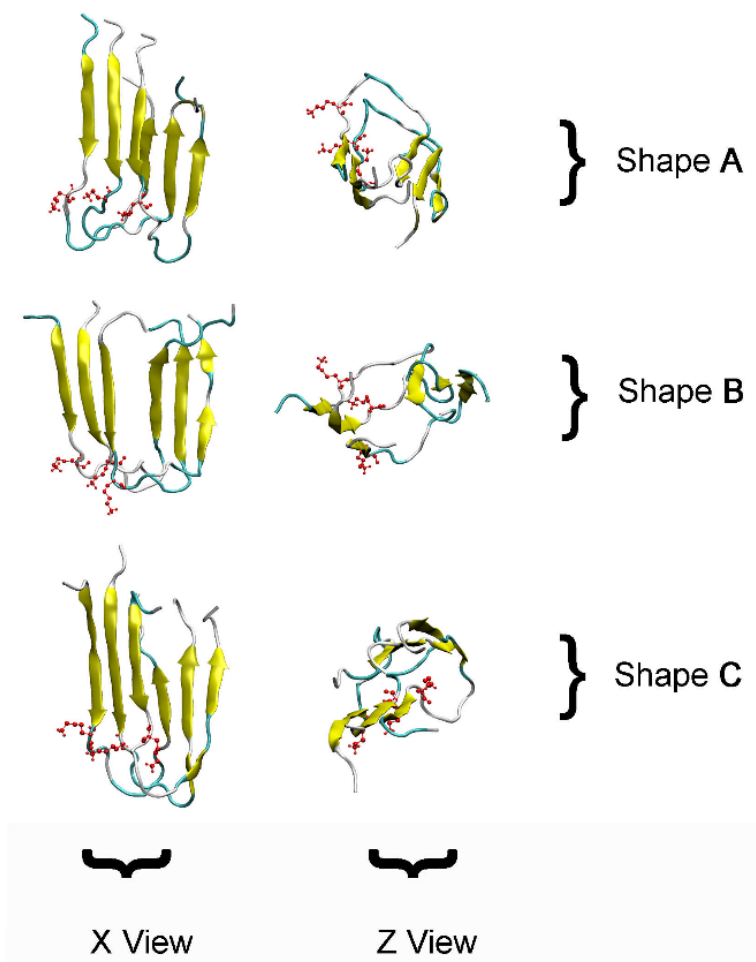


Fig. 5. Representative conformations of tmE22K 3A β_{11-40} were obtained from FEL and clustering analysis.

Table 3. Details of optimized structures of tmE22K 3A β_{11-40} .

Shape	R_g (nm)	SA (nm ²)	CCS (nm ²)	β -content (%)	Population (%)
A	1.51	67.31	13.72	40	37
B	1.59	79.34	15.46	40	25
C	1.53	70.76	14.34	44	16

III.4. Contacts of A β chain with other chains and DPPC lipid bilayer

We may argue that the interaction between neighboring chains of *tmE22K* trimer is more rigid than that of *tmWT* system due to forming larger amounts of SC and HB contacts each other.

In details, the intermolecular SC contact between constituting chains of E22K $3A\beta_{11-40}$ is computed as of 46.2 ± 5.0 that is seriously larger than that of WT system (42.7 ± 4.1). It is in good agreement with intermolecular hydrogen bond contact evaluations. There are of 16.5 ± 1.6 HB contacts that have been observed between neighboring chains of *tm*E22K $3A\beta_{11-40}$. The amount is significantly larger than that of *tm*WT trimer with the value of 10.5 ± 1.6 . Because the stronger contacts probably enhance the $A\beta$ self-aggregate [48], it may be argued that the formation rate of the trimer is probably boosted when the mutation is induced [44, 49].

The interaction of transmembrane protein and lipid bilayer is often considered as the intermolecular SC contacts between non-hydrogen atoms of individual residues of *tm*E22K trimer to phosphorus atoms of DPPC lipid bilayer [28]. The metric was calculated over the time interval 150-400 ns of REMD simulation at 324 K. The SC contact is available when the distance between two atoms is smaller than 4.5 Angstrom. The probability of the contact is shown in Fig. 6 in comparison with the available value of transmembrane WT $3A\beta_{11-40}$ [28]. Interestingly, the interacted picture has changed when the E22K mutation is induced. The number of contacts is significantly increased. As observed in WT system [28], the residues 11, 16, and 28 rigidly form SC to the membrane, however, the residue E22 has no contact to the phosphorus atoms. In the *tm*E22K system, these residues are found to be able to adopt more rigid SC to the DPPC membrane. Moreover, the residue K22 absolutely forms connections with the membrane surface. Overall, the *tm*E22K $3A\beta_{11-40}$ probably adopts a stronger interaction to the DPPC membrane than *tm*WT trimer does. Thus, the *tm*E22K $3A\beta_{11-40}$ is seemingly easier than the WT form in self-insert into the membrane.

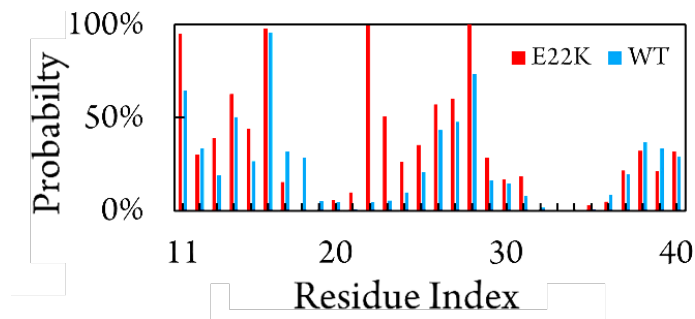


Fig. 6. The probability of intermolecular SC contact between non-hydrogen atoms of *tm*E22K and *tm*WT (imitated from Ref [28] with permission of the Royal Society of Chemistry) trimer to the phosphorus atoms of DPPC lipid bilayer.

IV. Stable of DPPC membrane during computation

The stability of the DPPC membrane lipid bilayer is investigated throughout the calculation of lipid order specifications. In particular, the lipid order parameter was calculated over the interval 150-400 ns of REMD simulation at 324 K. The obtained metrics are noted with red and black colors in Fig. 7 that are in good agreement with the previous studies in both computations and experiments [27, 28, 50–52]. The observed curves are different from the pure lipid system (reported in Ref. [28]). The difference implies the influence of transmembrane $A\beta$ peptides on the DPPC membrane lipid bilayer. However, overall, the membrane is durable during the computations.

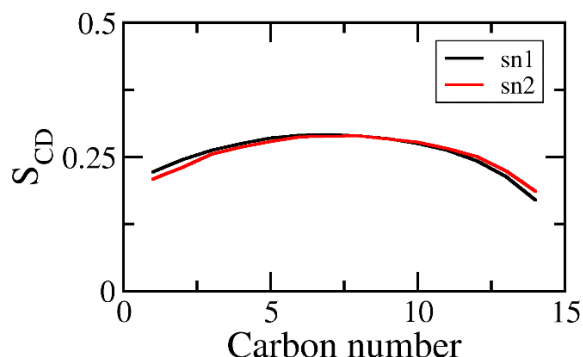


Fig. 7. Lipid order specifications of both carbon atoms of acyl chains sn1 and sn2.

V. CONCLUSIONS

The E22K mutation was found to increase the size of the transmembrane $3A\beta_{11-40}$ peptide. The secondary structure records are significantly changed, in which, the β -content is increased but other metrics are decreased. The *tmE22K* $3A\beta_{11-40}$ forms more intermolecular contacts (both SC and HB) between establishing chains. It is mentioned that the binding affinity between constituting chains of trimer is enhanced, thus the fibril formation rate is probably boosted [48]. The momentous gain of intermolecular contacts with DPPC molecules implies that *tmE22K* $3A\beta_{11-40}$ would be self-inserted more easily into the membrane than the WT form. All of *tmE22K* $3A\beta_{11-40}$ optimized structures adopt U-shape structural style. The sequences fully penetrate the membrane forming the β -structure, while the sequences located on the membrane surface adopt the coil structure. Overall, the *in silico* study indicates that the E22K mutation alters $3A\beta_{11-40}$ to be larger, more stable and have stronger interaction with DPPC membrane lipid bilayer. The results are in good agreement with experiments that E22K amyloid faster self-aggregates [44].

ACKNOWLEDGEMENTS

The work is funded by Vietnam National Foundation for Science & Technology Development (NAFOSTED) under the grant number 103.01-2016.48.

REFERENCES

- [1] H. W. Querfurth and F. M. LaFerla, *N. Engl. J. Med.* **362** (2010) 329.
- [2] Alzheimer's association, Alzheimer's disease facts and figures Alzheimer's disease facts and figures (2016).
- [3] M. D. Carter, G. A. Simms, D. F. Weaver, *Clinical Pharmacology and Therapeutics* **88** (2010) 475.
- [4] J. Nasica-Labouze, P. H. Nguyen, F. Sterpone, O. Berthoumieu, N.-V. Buchete, S. Coté, A. De Simone, A. J. Doig, P. Faller, A. Garcia, A. Laio, M. S. Li, S. Melchionna, N. Mousseau, Y. Mu, A. Paravastu, S. Pasquali, D.J. Rosenman, B. Strodel, B. Tarus, J.H. Viles, T. Zhang, C. Wang and P. Derreumaux, *Chem. Rev.* **115** (2015) 3518.
- [5] L. M. Jarvis, *Chem. Eng. News* **90** (2012) 8.
- [6] D.J. Selkoe, J. Hardy, *EMBO Mol. Med.* **8** (2016) 595.
- [7] W. I. Rosenblum, *Neurobiol Aging* **35**(2004) 969.
- [8] A. Abbott and E. Dolgin, *Nature* **540** (2016) 15.
- [9] A. J. Doig, M. P. del Castillo-Frias, O. Berthoumieu, B. Tarus, J. Nasica-Labouze, F. Sterpone, P. H. Nguyen, N. M. Hooper, P. Faller, P. Derreumaux, *ACS Chem. Neurosci.* **8** (2017) 1435.
- [10] D. M. Walsh and D. J. Selkoe, *J. Neurochem.* **101** (2007) 1172.

- [11] J. Bieschke, M. Herbst, T. Wiglenda, R.P. Friedrich, A. Boeddrich, F. Schiele, D. Kleckers, J.M. Lopez del Amo, B.A. Grüning, Q. Wang, M.R. Schmidt, R. Lurz, R. Anwyl, S. Schnoegl, M. Fändrich, R.F. Frank, B. Reif, S. Günther, D. M. Walsh and E. E. Wanker, *Nat. Chem. Biol.* **8**(2012) 93.
- [12] M. K. Jana, R. Cappai, C. L. L. Pham and G. D. Ciccotosto, *J. Neurochem.* **136**(2016) 594.
- [13] S. Banerjee, Z. Sun, E.Y. Hayden, D.B. Teplow and Y. L. Lyubchenko, *ACS Nano* **11** (2017) 12202.
- [14] S. T. Ngo, S.-T. Fang, S.-H. Huang, C.-L. Chou, P.D.Q. Huy, M.S. Li and Y.-C. Chen, *J. Chem. Inf. Model.* **56** (2016) 1344.
- [15] L. Tran, S. T. Ngo and M. T. Nguyen, *Chem. Phys. Lett.* **696**(2018) 55.
- [16] L. Hendriks, C. M. van Duijn, P. Cras, M. Cruts, W. Van Hul, F. van Harskamp, A. Warren, M. G. McInnis, S. E. Antonarakis, J.-J. Martin, A. Hofman and C. Van Broeckhoven, *Nat. Genet* **1** (1992) 218.
- [17] E. Levy, M. Carman, I. Fernandez-Madrid, M. Power, I. Lieberburg, S. van Duinen, G. Bots, W. Luyendijk and B. Frangione, *Science* **248**(1990) 1124.
- [18] C. Nilsberth, A. Westlind-Danielsson, C.B. Eckman, M.M. Condrón, K. Axelman, C. Forsell, C. Stenh, J. Luthman, D.B. Teplow, S.G. Younkin, J. Naslund and L. Lannfelt, *Nat. Neurosci.* **4** (2001) 887.
- [19] T. Tomiyama, T. Nagata, H. Shimada, R. Teraoka, A. Fukushima, H. Kanemitsu, H. Takuma, R. Kuwano, M. Imagawa, S. Ataka, Y. Wada, E. Yoshioka, T. Nishizaki, Y. Watanabe and H. Mori, *Ann. Neurol.* **63** (2008) 377.
- [20] T. J. Grabowski, H. S. Cho, J. P. G. Vonsattel, G. W. Rebeck and S. M. Greenberg, *Ann. Neurol.* **49** (2001) 697.
- [21] O. Bugiani, A. Padovani, M. Magoni, G. Andora, M. Sgarzi, M. Savoirdo, A. Bizzi, G. Giaccone, G. Rossi and F. Tagliavini, *Neurobiol. Aging*, **19** (1998) S238.
- [22] S.-H. Chong, J. Yim, S. Ham, Structural heterogeneity in familial Alzheimer's disease mutants of amyloid-beta peptides, *Mol. BioSyst.*, **9** (2013) 997.
- [23] N. Sureshbabu, R. Kirubakaran, H. Thangarajah and E. J. P. Malar, R. Jayakumar, *J. Mol. Neurosci.* **41** (2010) 368.
- [24] A. Quist, I. Doudevski, H. Lin, R. Azimova, D. Ng, B. Frangione, B. Kagan, J. Ghiso, R. Lal, Amyloid Ion Channels: A Common Structural Link for Protein-Misfolding Disease, *Proc. Natl. Acad. Sci. U.S.A.* **102** (2005) 10427-10432.
- [25] T. L. Williams and L. C. Serpell, *FEBS J.* **278** (2011) 3905.
- [26] L. Connelly, H. Jang, F. Teran Arce, R. Capone, S.A. Kotler, S. Ramachandran, B.L. Kagan, R. Nussinov and R. Lal, *J. phys. Chem. B* **116** (2012) 1728.
- [27] S. T. Ngo, M. T. Nguyen, N. T. Nguyen and V. V. Vu, *J. Phys. Chem. B* **121** (2017) 8467.
- [28] S. T. Ngo, H. M. Hung, K. N. Tran and M. T. Nguyen, *RSC Adv.* **7** (2017) 7346.
- [29] I. Bertini, L. Gonnelli, C. Luchinat, J. Mao and A. Nesi, *J. Am. Chem. Soc.* **133** (2011) 16013.
- [30] P. Schrödinger LLC, The PyMOL molecular graphics system, Version 1.3r1, 2010.
- [31] C. Oostenbrink, A. Villa, A.E. Mark and W.F. Van Gunsteren, *J. Comput. Chem.*, **25** (2004) 1656.
- [32] J. F. Nagle, *Biophys. J.* **64** (1993) 1476.
- [33] H. J. C. Berendsen, J. P. M. Postma, W. F. van Gunsteren, a.J. Hermans, *Intermolecular Forces*, Reidel, Dordrecht, Jerusalem, Israel, 1981.
- [34] S. Côté, R. Laghaei, P. Derreumaux and N. Mousseau, *J. Phys. Chem. B* **116** (2012) 4043.
- [35] B. Tarus, T. T. Tran, J. Nasica-Labouze, F. Sterpone, P. H. Nguyen and P. Derreumaux, *J. Phys. Chem. B* **119** (2015) 10478.
- [36] S. T. Ngo, H. M. Hung, D. T. Truong and M. T. Nguyen, *Phys. Chem. Chem. Phys.* **19** (2017) 1909-1919.
- [37] S. T. Ngo, X.-C. Luu, M. T. Nguyen, C. N. Le and V. V. Vu, *RSC Adv.* **7** (2017) 42379.
- [38] M. J. Abraham, T. Murtola, R. Schulz, S. Páll, J. C. Smith, B. Hess, E. Lindahl, *SoftwareX* **1-2**(2015) 19.
- [39] W. G. Touw, C. Baakman, J. Black, T. A. H. te Beek, E. Krieger, R. P. Joosten and G. Vriend, *A Nucleic Acids Res.* **43**(2015) D364.
- [40] Erik G. Marklund, Matteo T. Degiacomi, Carol V. Robinson, Andrew J. Baldwin and Justin L.P. Benesch, *Structure* **23** (2015) 791.
- [41] E. Papaleo, P. Mereghetti, P. Fantucci, R. Grandori and L. De Gioia, *J. Mol. Graph. Model.*, **27** (2009) 889.
- [42] Z. Qian, Q. Zhang, Y. Liu and P. Chen, *PLOS ONE*, **12** (2017) e0188794.
- [43] S. T. Ngo, H. M. Hung, N. D. Hong and N. T. Tung, *J Mol. Graph. Model.*, **83** (2018) 122-128.
- [44] X. Yang, G. Meisl, B. Frohm, E. Thulin, T. P. J. Knowles and S. Linse, On the role of sidechain size and charge in the aggregation of A beta 42 with familial mutations, *Proc. Nat. Acad. Sci. U S A* **115** (2018) E5849.

- [45] Y. Fezoui and D. B. Teplow, *J. Biol. Chem.* **277** (2002) 36948.
- [46] E. Papaleo, P. Mereghetti, P. Fantucci, R. Grandori and L. De Gioia, *J. Mol. Graph. Model* **27** (2009) 889-899.
- [47] S. T. Ngo, D. T. Truong, N. M. Tam, M. T. Nguyen, *J. Mol. Graph. Model.* **76** (2017) 1.
- [48] M. Kouza, A. Banerji, A. Kolinski, I. Buhimschi, A. Kloczkowski, Relationships between Mechanostability, Aggregation Rate and Binding Affinity of Peptides: Insights from All-ATOM Modeling in Explicit Solvent, *Biophys. J.*, **110** (2016) 386a.
- [49] M. H. Viet, P. H. Nguyen, S. T. Ngo, M. S. Li and P. Derreumaux, *ACS Chem Neurosci.* **4** (2013) 1446.
- [50] H. I. Petrache, S. W. Dodd, M. F. Brown, *Biophys. J.* **79**(2000) 3172.
- [51] D. P. Tieleman, S. J. Marrink, H. J. C. Berendsen, *Biomembranes* **1331** (1997) 235.
- [52] H. M. Hung, V. P. Nguyen, S. T. Ngo, M. T. Nguyen, *BioPhys. Chem.* **217** (2016) 1.